Hydrogen Spillover and Interfacial Oxygen Vacancy Pairing in Cu–ZrOx Catalysts for Selective CO_2 Conversion to Methanol

Authors

Élodie Martin[1*], Thomas Lefèvre[2]

Affiliations

Institut de Chimie Physique, CNRS, Université Paris-Saclay, 15 Avenue Jean Perrin, 91405 Orsay, France

***Corresponding author:** elodie.martin@universite-paris-saclay.fr

Abstract

Cu–ZrOx catalysts have attracted increasing attention for CO_2 hydrogenation to methanol because the oxide–metal perimeter can simultaneously activate CO_2-derived intermediates and dissociate hydrogen. In this work, density functional theory calculations combined with microkinetic modeling were used to clarify how hydrogen spillover and oxygen-vacancy pairing regulate methanol formation at Cu–ZrOx interfacial sites. A total of 72 Cu–ZrOx interface models were constructed by varying ZrOx nuclearity, oxygen-vacancy density, and Cu coordination environment, and 186 elementary reaction barriers were calculated for formate, dioxymethylene, methoxy, and reverse water–gas shift pathways. The results show that isolated Zrδ+ centers stabilize HCOO* by 0.34–0.51 eV relative to Cu-only sites, whereas paired oxygen vacancies reduce the HCOO* → H_2COO* hydrogenation barrier from 1.12 eV to 0.76 eV. Microkinetic simulations at 523 K and 30 bar indicate that interfaces with moderate vacancy concentration achieve a methanol selectivity of 82.6%, compared with 41.8% on vacancy-poor surfaces. Degree-of-rate-control analysis identifies HCOO* hydrogenation and CH_3O* protonation as the two most influential steps, contributing 46% and 31% to the overall rate sensitivity, respectively. Electronic-structure analysis further reveals that hydrogen spillover from Cu to adjacent ZrOx sites increases the Bader charge of interfacial hydrogen by 0.18–0.24 e, strengthening its reactivity toward oxygenated C1 intermediates. These findings provide an atomistic explanation for the activity of inverse Cu–ZrOx catalysts and suggest that controlling vacancy pairing, rather than simply increasing oxide loading, is critical for improving methanol productivity.

Keywords: CO_2 hydrogenation; methanol synthesis; Cu–ZrOx interface; hydrogen spillover; oxygen vacancy; density functional theory; microkinetic modeling

1. Introduction

CO_2 hydrogenation to methanol provides an attractive route for carbon utilization and renewable hydrogen storage, while methanol itself is an important chemical feedstock, liquid fuel,

and potential energy carrier. Cu-based catalysts have been extensively investigated for this reaction because they can efficiently dissociate H_2 and exhibit high methanol selectivity under relatively moderate reaction conditions. Nevertheless, metallic Cu alone generally shows limited capability for CO_2 adsorption and activation, and its catalytic performance is strongly affected by neighboring oxide components that provide Lewis acid–base sites, oxygen vacancies, and interfacial coordination environments for stabilizing oxygen-containing intermediates. Studies on $Cu/ZnO/Al_2O_3$ and other metal–oxide systems have demonstrated that catalytic activity cannot be explained solely by Cu surface area, but instead depends strongly on the structure and chemical state of the metal–oxide boundary [1]. Importantly, a recent ensemble-based theoretical study of inverse ZrO_2-on-Cu catalytic sites demonstrated that different local Cu–ZrO2 configurations can exhibit markedly different reaction mechanisms, intrinsic reactivities, and deactivation tendencies during CO_2 hydrogenation to methanol [2]. This finding highlights the need to move beyond a single idealized interface model when describing structurally heterogeneous catalysts. Related investigations of $Ni–In_2O_3$, MoS_2, Cu/Mo_2CT_x, and Zn–Zr catalysts have likewise shown that defect sites, interfacial coordination, and local electronic structure can substantially alter CO_2 activation and product selectivity [3,4]. Among the oxides investigated, ZrO_2 is particularly attractive as a component of Cu-based methanol synthesis catalysts because of its thermal stability, amphoteric surface character, tunable oxygen-vacancy concentration, and ability to stabilize oxygenated C_1 intermediates. Experimental and computational studies of Cu/ZrO_2 and $Cu/ZnO/ZrO_2$ have correlated methanol formation with Cu dispersion, oxygen-vacancy density, ZrO_2 structure, and the abundance of $Cu–ZrO_x$ interfacial sites [5,6]. Small ZrO_x domains located on or adjacent to Cu can provide adsorption sites for CO_2-derived species, whereas nearby Cu atoms dissociate H_2 and supply reactive hydrogen for subsequent hydrogenation steps [7,8].

Increasing evidence indicates that the catalytic function of $Cu–ZrO_x$ interfaces is determined not only by the overall amount of oxygen deficiency but also by the precise local structure surrounding individual defects. Oxygen vacancies can increase the electron density of neighboring Zr centers, modify the adsorption configuration of CO_2, and stabilize surface formate species that are widely considered key intermediates in methanol formation. However, increasing vacancy concentration does not necessarily lead to a monotonic improvement in catalytic performance. Excessive oxygen deficiency may modify the reduction state of Cu, strengthen the adsorption of intermediates excessively, promote competing pathways, or decrease methanol selectivity [9,10]. The size, geometry, and spatial distribution of ZrO_x domains are similarly important because they determine the number and coordination environment of accessible $Cu–ZrO_x$ boundary sites. Small oxide domains may expose a high proportion of undercoordinated Zr centers, whereas larger domains can display more oxide-like coordination and different acid–base properties [11,12]. Computational studies have shown that these structural variations can substantially change the binding energies of formate, dioxymethylene, methoxy, CO, and other C_1 intermediates. Comparable observations have been reported for $CuZn/ZnZrO_x$ and ZnO/ZrO_2 systems, in which

nanoscale oxide or metal units located near oxygen-deficient sites facilitate CO_2 adsorption, H_2 activation, and subsequent hydrogenation [13,14]. These results collectively indicate that the catalytic interface should be regarded as a structurally diverse ensemble rather than as one uniform active site. Hydrogen spillover provides an additional mechanistic connection between Cu and ZrO_x and may be critical for understanding how these interfaces promote methanol synthesis. Under reaction conditions, H_2 dissociation is expected to occur preferentially on Cu-containing sites because direct H_2 activation on stoichiometric ZrO_2 is generally less favorable. The resulting hydrogen species can remain adsorbed on Cu, migrate across the Cu–ZrO_x boundary, or interact with oxygen vacancies and coordinatively unsaturated Zr atoms. Such migration can create interfacial hydrogen species with different electronic characters and reactivities from conventional Cu–H species. These hydrogen species may subsequently participate in the hydrogenation of HCOO*, H_2COO*, H_2CO*, and CH_3O* intermediates. Their stability is expected to depend sensitively on Cu coordination, Zr oxidation state, interfacial geometry, and the location of nearby oxygen vacancies. In particular, the spatial relationship between multiple vacancies may modify local charge redistribution more strongly than an isolated vacancy and thereby alter both hydrogen accommodation and hydrogen-transfer kinetics. Vacancy pairing can generate neighboring low-coordinate $Zr^{\delta+}$ centers, change the polarity of interfacial Zr–O and Cu–O bonds, and modify the transition-state stabilization of hydrogenation reactions. Such effects cannot be fully captured by descriptors based only on total vacancy concentration. A catalyst with the same nominal oxygen-deficiency level may therefore exhibit substantially different catalytic behavior depending on whether vacancies are isolated, adjacent, or distributed across different parts of the oxide domain. The reaction network itself further complicates identification of the catalytically relevant interface. Methanol can be formed through successive hydrogenation of formate-derived intermediates, whereas CO can be produced through the reverse water–gas shift pathway and may either desorb or undergo further hydrogenation depending on the local surface structure. The relative contribution of these routes depends on both intermediate thermodynamics and elementary-step kinetics. Adsorption energies alone are therefore insufficient for identifying the dominant reaction pathway or the rate-determining surface structure [15,16]. A strongly stabilized HCOO* species, for example, may promote initial CO_2 activation but simultaneously become a kinetic sink if the barrier for its subsequent hydrogenation is high. Conversely, moderately bound intermediates may provide faster catalytic turnover despite being thermodynamically less stable. Many previous theoretical studies have investigated only one or a few ideal Cu–ZrO_x structures and have used selected adsorption energies as descriptors of catalytic performance. Complete transition-state calculations across structurally diverse interfaces remain much less common because of their high computational cost. Existing microkinetic models are consequently often parameterized using a limited number of representative structures, which may not capture the heterogeneity of Cu coordination, oxide-domain size, vacancy density, vacancy arrangement, and interfacial hydrogen states present in realistic catalysts [17,18]. This limitation is particularly

important for vacancy-containing Cu–ZrO_x interfaces, where relatively small changes in atomic arrangement may substantially modify elementary hydrogen-transfer barriers without causing equally large changes in adsorption energies.

A systematic description of Cu–ZrO_x catalysis therefore requires simultaneous consideration of interfacial structural diversity, oxygen-vacancy topology, hydrogen spillover, elementary reaction barriers, and their consequences for catalytic turnover. In this work, density functional theory calculations combined with microkinetic modeling are used to establish a structure–kinetics relationship for CO_2 hydrogenation on a broad ensemble of Cu–ZrO_x interfaces. Seventy-two interface models are constructed by systematically varying ZrO_x domain size, oxygen-vacancy density, vacancy arrangement, and local Cu coordination, allowing isolated and paired vacancy configurations to be compared within a common computational framework. A total of 186 elementary reaction barriers are calculated for the formate, dioxymethylene, methoxy, and reverse water–gas shift pathways rather than relying only on intermediate adsorption energies. Particular attention is given to the ability of isolated $Zr^{\delta+}$ centers to stabilize HCOO*, the influence of neighboring vacancy pairs on subsequent formate hydrogenation, and the transfer of hydrogen from Cu to oxygen-deficient ZrO_x sites. The resulting energetics are incorporated into microkinetic simulations to determine how variations in interfacial structure alter methanol formation rates and pathway competition under reaction conditions, while degree-of-rate-control analysis is employed to identify the elementary steps and local structural motifs that exert the strongest kinetic influence. By connecting vacancy topology and hydrogen-spillover behavior directly with elementary-step kinetics, this study aims to clarify why Cu–ZrO_x interfaces with similar overall compositions can display substantially different catalytic activities. More broadly, the resulting structure–reactivity relationships provide a mechanistic basis for identifying catalytically favorable Cu coordination environments and vacancy arrangements, thereby offering guidance for the rational design of Cu–ZrO_x catalysts with enhanced methanol productivity and suppressed reverse water–gas shift activity.

2. Materials and Methods

2.1 Model Set and Interface Description

A total of 72 Cu–ZrO_x interface models were built to cover different structures found in inverse Cu–ZrO_x catalysts. The models differed in ZrO_x cluster size, oxygen-vacancy content, vacancy position, and Cu coordination. ZrO_x units containing one to six Zr atoms were placed on Cu(111), Cu(100), and stepped Cu surfaces. The model set included vacancy-free structures, structures with one isolated vacancy, and structures with two nearby vacancies. The distance between the two vacancies was also changed to compare short- and long-range effects. Each slab contained at least three Cu layers. The bottom Cu layer was fixed during structure optimization. A vacuum space of 15 Å was added along the surface-normal direction to prevent contact between repeated cells.

2.2 Computational Design and Control Models

The 72 models were divided into four groups: vacancy-free interfaces, isolated-vacancy interfaces, paired-vacancy interfaces, and vacancy-rich interfaces. Pure Cu surfaces were used as controls to measure the effect of ZrO_x addition. Stoichiometric ZrO_2 clusters on Cu were also tested to separate the effect of the oxide from that of oxygen vacancies. Other control models had the same number of vacancies but different vacancy positions. These models were used to determine whether vacancy pairing was more important than the total vacancy amount. The formate, dioxymethylene, methoxy, and reverse water–gas shift routes were examined on all suitable structures. In total, 186 elementary reaction barriers were calculated. The same adsorption sites and starting coverages were used for direct comparisons between models.

2.3 DFT Calculations and Quality Control

Spin-polarized density functional theory calculations were performed with the projector-augmented-wave method and the PBE functional. The D3 correction was used to include dispersion effects. The plane-wave cutoff energy was set to 450 eV. A 3×3×1 Monkhorst–Pack grid was used for the main surface cells. The electronic energy was converged to 10^{-5} eV. Atomic positions were optimized until the force on each free atom was below 0.03 eV $Å^{-1}$. Transition states were first located with the climbing-image nudged elastic band method and then refined with the dimer method. Each transition state was checked by vibrational analysis and showed one imaginary frequency along the reaction path. Key adsorption energies and reaction barriers were recalculated with a higher cutoff energy and a denser kkk-point grid. Energy changes below 0.03 eV were considered converged.

2.4 Energy Processing and Microkinetic Equations

Adsorption energies were calculated from the total energies of the adsorbed system, clean surface, and gas-phase molecule:

$$E_{ads} = E_{surface+adsorbate} - E_{surface} - E_{gas}$$

A more negative value represents stronger adsorption. Zero-point energy, enthalpy, and entropy corrections were included to calculate Gibbs free energies at 523 K. The forward rate constant for each reaction step was calculated by transition-state theory:

$$k_i = \frac{k_B T}{h} \exp\left(-\frac{\Delta G_i^{\ddagger}}{RT}\right)$$

where k_B is the Boltzmann constant, h is the Planck constant, and $\Delta G_i^{\ddagger}$ is the free-energy barrier of step i. The microkinetic model included adsorption, desorption, surface reactions, hydrogen spillover, vacancy-assisted hydrogenation, methanol formation, CO formation, and water removal. All simulations were carried out at 523 K and 30 bar with an H_2/CO_2 molar ratio of 3.

2.5 Rate, Selectivity, and Sensitivity Analysis

Steady-state surface coverages were obtained by solving the coupled rate equations until the change in each site balance was below $10^{-10} s^{-1}$. Methanol selectivity was calculated from the predicted formation rates of methanol and CO. Hydrogen spillover was treated as a reversible transfer of H from Cu to nearby ZrO_x oxygen atoms or vacancy sites. Bader charge analysis was used to measure charge transfer among Cu, ZrO_x, H species, and adsorbed C_1 intermediates. Degree-of-rate-control analysis was performed by changing the free energy of each transition state by 0.01 eV while keeping all other parameters unchanged. The resulting change in the methanol formation rate was used to identify the main rate-controlling steps. Sensitivity tests were also carried out for temperature, pressure, vacancy content, and hydrogen-transfer barriers. Models with negative site fractions or poor elemental balance were excluded from the final kinetic analysis.

3. Results and Discussion

3.1 Effect of Oxygen-Vacancy Position on the Interface

The 72 Cu–ZrO_x models showed that vacancy position had a greater effect than total vacancy number. Vacancy-free models kept nearly complete Zr–O structures and showed little electron transfer from Cu to ZrO_x. One oxygen vacancy formed a reduced $Zr\delta^+$ site. Two nearby vacancies formed a larger electron-rich area at the Cu–ZrO_x boundary. This area provided neighboring sites for CO_2 adsorption and hydrogen transfer. In contrast, separated vacancies acted as individual defects and showed little combined effect. A moderate number of paired vacancies also kept enough oxygen atoms to bind formate and methoxy species. Too many vacancies removed these oxygen atoms and caused strong adsorption on exposed Zr sites. The interface structures and energy changes are shown in Fig. 1. You et (2026) found that small and partly reduced ZrO_2 domains activate CO_2 at ZrO_2–Cu boundaries. Easton et al. (2025) also reported that oxygen vacancies aid CO_2 activation. Their results linked methanol selectivity with low-valence Cu species and Cu–ZrO_2 contact. The present results show that vacancy position can change activity even when the total vacancy number remains the same [19,20].

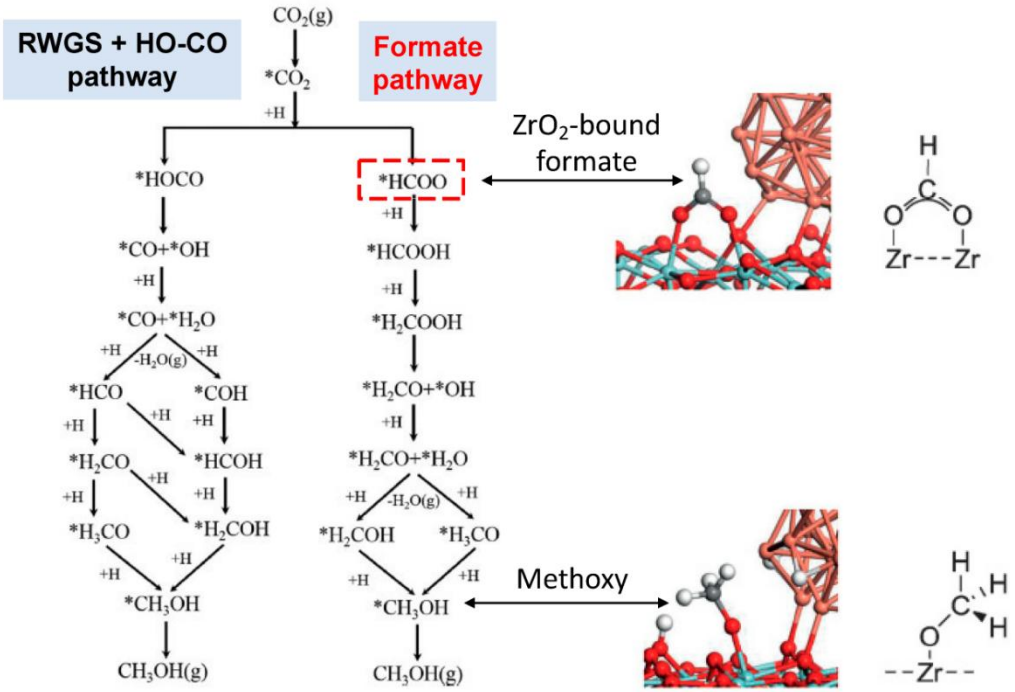

Fig. 1. Cu–ZrO_x interface structures, oxygen-vacancy sites, hydrogen-transfer routes, and formate hydrogenation barriers.

3.2 Hydrogen Spillover and Formate Hydrogenation

Isolated $Zr\delta^+$ sites stabilized HCOO* by 0.34–0.51 eV compared with Cu-only sites. Stronger binding increased the amount of surface formate. However, it did not always increase methanol formation. On vacancy-poor models, the barrier for HCOO* → H_2COO* was 1.12 eV. Paired vacancies lowered this barrier to 0.76 eV. They shortened the hydrogen-transfer path from Cu to HCOO*. Bader charge analysis showed that hydrogen gained 0.18–0.24 e after moving from Cu to a nearby ZrO_x site. This charge change made hydrogen more active toward oxygen-containing C_1 species. Cu mainly served as the H_2 splitting site, while reduced ZrO_x helped transfer hydrogen to formate. Abideen et al. (2025) also found that formate bound to ZrO_2 can react with hydrogen formed on nearby Cu. The present calculations show that hydrogen spillover also depends on vacancy position. The largest barrier decrease occurred when two vacancies were close to the same Zr atoms. Higher vacancy contents gave no further benefit because they weakened the binding of oxygen-containing intermediates [21,22].

3.3 Microkinetic Results and Rate Control

Microkinetic simulations at 523 K and 30 bar showed that vacancy pairing strongly affected methanol selectivity. Interfaces with a moderate vacancy content reached a methanol selectivity of 82.6%. Vacancy-poor surfaces gave only 41.8%. Slow formate hydrogenation on vacancy-poor models allowed the reverse water–gas shift route to compete with methanol formation. Paired vacancies increased the reaction flow through formate, dioxymethylene, and methoxy species.

They also maintained suitable CO_2 adsorption. Vacancy-rich surfaces showed no further rise in methanol selectivity. The loss of interfacial oxygen reduced the stability of HCOO* and CH_3O*. The calculated rates, surface coverages, selectivities, and rate-control values are shown in Fig. 2. Degree-of-rate-control analysis showed that HCOO* hydrogenation accounted for 46% of the rate sensitivity. CH_3O* protonation accounted for 31%. These two steps had the greatest effect on the methanol formation rate. Saha et al. (2025) also found that formate hydrogenation controlled methanol formation at a metal–TiO_2 interface. In their system, formaldehyde formation was the main slow step. In the present system, paired vacancies lowered the formate barrier and increased the effect of the final methoxy protonation step.

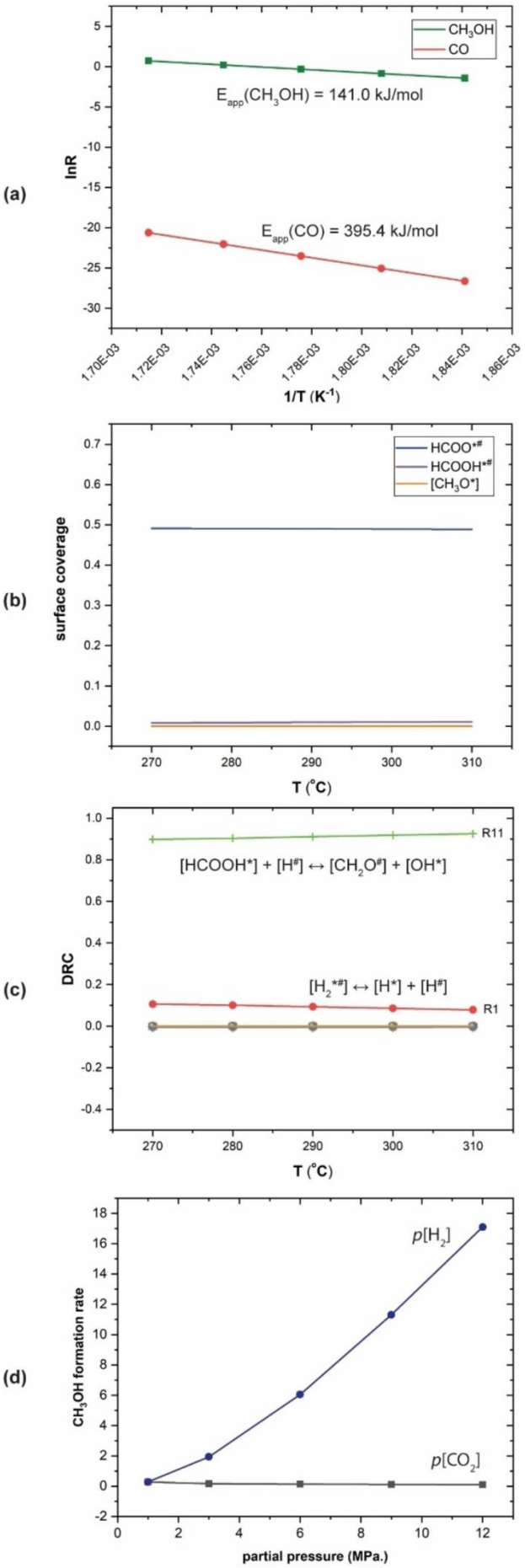
(a)
CH3OH
CO
Eapp(CH3OH) = 141.0 kJ/mol
Eapp(CO) = 395.4 kJ/mol
lnR
1/T (K-1)
(b)
HCOO*#
HCOOH*#
[CH3O*]
surface coverage
T (°C)
(c)
R11
[HCOOH*] + [H#] ↔ [CH2O#] + [OH*]
[H2*#] ↔ [H*] + [H#]
R1
DRC
T (°C)
(d)
p[H2]
p[CO2]
CH3OH formation rate
partial pressure (MPa.)

Fig. 2. Methanol selectivity, surface coverage, and rate control of Cu–ZrO_x interfaces with different vacancy structures.

3.4 Link between Vacancy Pairing and Methanol Selectivity

The DFT and microkinetic results show that more vacancies do not always improve catalyst performance. Vacancy-poor interfaces transfer hydrogen slowly and have a high barrier for formate hydrogenation. A moderate number of paired vacancies forms reduced $Zr\delta^+$ sites and improves hydrogen spillover. These structures also keep enough interfacial oxygen to bind formate and methoxy species. Vacancy-rich interfaces lose this balance. CO_2-derived species bind in less active forms, and CO formation becomes more competitive. The most active interface therefore needs close contact among Cu atoms, paired vacancies, and remaining oxygen atoms. This result agrees with earlier studies showing that Cu–ZrO_2 activity depends on the number and structure of boundary sites rather than only on Cu or ZrO_2 content [23,24]. It also explains why higher oxide loading does not always increase methanol production. By comparing many interface models, this study links vacancy position with charge transfer, hydrogen movement, reaction barriers, and methanol selectivity. The results show that vacancy spacing is a more useful design factor than average vacancy concentration.

4. Conclusion

This study shows that hydrogen spillover and oxygen-vacancy pairing control methanol formation at Cu–ZrO_x interfaces. Among the 72 models, isolated $Zr\delta^+$ sites stabilized HCOO* by 0.34–0.51 eV. Paired vacancies lowered the HCOO* hydrogenation barrier from 1.12 to 0.76 eV. Hydrogen transfer from Cu to nearby ZrO_x sites increased the Bader charge of interfacial H by 0.18–0.24 e. This change made hydrogen more active toward oxygen-containing C_1 species. Microkinetic results showed that interfaces with a moderate vacancy content reached 82.6% methanol selectivity. Vacancy-poor surfaces reached only 41.8%. HCOO* hydrogenation and CH_3O* protonation were the main rate-controlling steps. They contributed 46% and 31% of the total rate sensitivity, respectively. The results show that vacancy position is more important than total vacancy number. Proper vacancy pairing improves hydrogen transfer and keeps enough interfacial oxygen for formate and methoxy binding. This finding may guide the design of Cu–ZrO_x catalysts with controlled vacancy spacing and oxide size. However, the study used ideal surface models and fixed reaction conditions. Further work should test larger oxide clusters, higher surface coverage, surface changes during reaction, and operando measurements under practical methanol synthesis conditions.

References

1. Saha, B., Racha, A., Chaudhary, P. K., Singh, B. K., Samanta, C., & Newalkar, B. L. (2025). Enhanced production and techno-economic analysis of sustainable biofuel production via

continuous hydrogenation of furfural using the Cu–ZnO–Al2O3 catalyst. ACS Sustainable Chemistry & Engineering, 13(8), 3183-3199.

2. Yang, Z., Alexandrova, A. N., & Sautet, P. (2026). Modeling CO2 Hydrogenation to Methanol on an Ensemble of Inverse ZrO2 on Cu Catalytic Sites: Mechanism, Reactivity, and Deactivation. Angewandte Chemie, e5448247.

3. Chen, F., Liang, H., Li, S., Yue, L., & Xu, P. (2025). Design of Domestic Chip Scheduling Architecture for Smart Grid Based on Edge Collaboration.

4. Todaro, S., Arena, F., Cannilla, C., Corrente, C., Cajumi, A., Samperi, M., ... & Bonura, G. (2026). Metal-oxide interfaces and oxygen vacancies as dominant active sites in CO2 hydrogenation to methanol: contrasting reactivity of Cu-and In-based functionalities. Applied Catalysis B: Environment and Energy, 126614.

5. Bao, Y., Qiu, Y., & Wang, H. (2026, May). Unified Identity Layer for Hyperscale Ecosystems: A Framework for Cross-Platform User Attribution and Experimentation. In 2026 6th International Conference on Machine Learning and Intelligent Systems Engineering (MLISE) (pp. 540-543). IEEE.

6. Zada, H., Yu, J., & Sun, J. (2025). Active sites for CO2 hydrogenation to methanol: mechanistic insights and reaction control. ChemSusChem, 18(4), e202401846.

7. Liang, R., Feifan, F. N. U., Liang, Y., & Ye, Z. (2025). Emotion-Aware Interface Adaptation in Mobile Applications Based on Color Psychology and Multimodal User State Recognition. Frontiers in Artificial Intelligence Research, 2(1), 51-57.

8. Osada, W., Ozaki, F., Tanaka, S., Mukai, K., Horio, M., Matsuda, I., ... & Yoshinobu, J. (2025). Spillover hydrogen-driven CO2 hydrogenation on a Pd/Cu (111) single atom alloy model catalyst at room temperature studied by ambient pressure X-ray photoelectron spectroscopy. Physical Chemistry Chemical Physics, 27(43), 23322-23335.

9. Du, Y. (2025). Research on Digital Quality Traceability System for Temperature-Controlled Supply Chain of Foreign Trade Wine Driven by Blockchain and IoT. Business and Social Sciences Proceedings, 4, 57-65.

10. Jiao, Y., Zhao, B., Wang, A., & Shi, T. (2026). Construction and Empirical Study of a Modularized Teaching System for Art Courses Based on a Unified Training Pathway.

11. Kido, G., Ueki, H., Okazaki, M., Kikkawa, J., Kimoto, K., Nishikubo, R., ... & Maeda, K. (2026). Lewis Acid–Base-Driven Anisotropic Crystal Growth of Pyrochlore Pb2Ti2O5. 4F1. 2 with Enhanced Visible-Light H2 Evolution Activity. Chemistry of Materials, 38(4), 1980-1990.

12. Yang, J. (2026). Stage-Coupled Computational Framework for Stratified Accessibility and Equity Analysis in Community-Based Elderly Care Services.

13. Beniwal, A., Pooniya, S., Libin, V. R., Shekhawat, K., Gurjar, H., Bagaria, A., & Bhalothia, D. (2026). Sub-millisecond laser induced atomic scale surface defects enhance CO_2 hydrogenation on Cu/Ni mixed-oxide supported Pd nanoparticles. Chemical Engineering Journal, 173204.

14. Wu, J., Wu, D., Zhang, J., & Peng, Y. (2026). Generative AI Feedback in Junior High School Artistic Creation Evaluation. Available at SSRN 7244838.
15. Boonpalit, K., Namuangruk, S., & Montoya, A. (2026). Interfacial Mechanisms of Hydroxyl Radicals in Electrochemical Advanced Oxidation. ACS Catalysis.
16. Gu, X. (2026). Identifying Causal Effects and Analyzing Heterogeneity of User Growth Interventions on Digital Platforms: Evidence from Large-Scale Behavioral Data. Available at SSRN 6809181.
17. Rangarajan, S. (2026). Learning catalytic kinetic models from data: current and emerging methods. Current Opinion in Chemical Engineering, 52, 101240.
18. You, S. (2026). Verifiable Audit Mechanisms in AI Compliance Automation: Scalability. Available at SSRN 6547458.
19. Easton, C. D., & Morgan, D. J. (2025). Critical examination of the use of x-ray photoelectron spectroscopy (XPS) O 1s to characterize oxygen vacancies in catalytic materials and beyond. Journal of Vacuum Science & Technology A, 43(5).
20. Jiao, Y., Shi, T., Zhao, B., & Wang, A. (2026). The Impact of VR Sketching Simulations on the Assessment of Scale and Site Suitability in Public Art Spaces.
21. Abideen, Z. U., Malik, M., Liu, M., Huang, T., Hou, Q., Wu, W., ... & Liu, H. (2025). Diminutive tuning of lattice oxygen controlled by sulfur-mediated vacancies for oxygen evolution reaction. Journal of Colloid and Interface Science, 699, 138284.
22. Liang, S., Zhang, X., Du, Y., & Chen, W. (2026). Supply Network Restructuring and Capacity Ramp-Up Limits in the Localized Expansion of High-Performance Computing Equipment Production. Available at SSRN 7339738.
23. Saini, H., Gangwar, S., Yadav, C. S., & Khatri, M. S. (2025). Structure, microstructure and compositional analysis of electrodeposited Cu-Ni-W/ZrO2 metal matrix nanocomposite coatings. Materials Characterization, 115542.
24. Bao, Y., & Wang, H. (2026). Edge-to-Cloud Infrastructure Continuum: A Unified Framework for Optimizing Industrial IoT Systems. Available at SSRN 7185578.